Plasmon enhanced fluorescence characteristics government by selecting the right objective function

M. Csete[1], D. Vass[1], A. Szenes[1], B. Bánhelyi[2], T. Csendes[2], G. Szabó[1]
1. Department of Optics and Quantum Electronics, University of Szeged, Dóm tér 9, Szeged 6720, Hungary
2. Department of Computational Optimization, University of Szeged, Árpád tér 2, Szeged 6720, Hungary

Abstract: Comparative study has been performed on concave spherical diamond-silver core-shell (SCS) and diamond-silver-diamond core-shell-shell (SCSS) nanoresonators consisting of four and six color centers, which were optimized to maximize the total fluorescence (P_x) and the corrected quantum efficiency (*cQE*) simultaneously. Our present study demonstrates that in plasmon enhanced non-cooperative fluorescence and in plasmonic superradiance optimization the right objective function is the P_x and P_x**cQE*, respectively.

Keywords: coupled plasmonic nanoresonator, fluorescence, superradiance, optimization

Introduction

If the illumination of a metal nanoparticle (NPs) occurs at the localized surface plasmon resonance (LSPR) wavelength, it results in a strong local EM-field enhancement. The wavelength of the resonance is specific to the material of the NP, and is sensitive to the size and shape of the nanoparticle [1].
Special types of plasmonic NPs are the concave core-shell (CS) nanoparticles. They consist of a dielectric core and a metal nanoshell. In case of CS NPs the energy of the plasmon modes depends on the ratio of inner radius corresponding to the core and to the outer radius of the shell (their difference is the shell thickness), as well as on the dielectric properties of the core and shell materials [2].
Diamond color centers are promising candidates as single-photon sources. These vacancy centers are important in quantum information processing, since they possess unpaired electron spin acting as a qubit [3]. Silicon vacancy centers (SiV) are the most promising diamond defects due to their stability, narrow fluorescence line, short lifetime and their unique orthogonal transitional dipole moments corresponding to the excitation and emission [4].
Superradiance is an intriguing phenomenon, which was predicted by Dicke [5]. In a two-level system, N atoms can exhibit N-times shorter radiative decay due to cooperativity, as a result the emission intensity is proportional to N^2 [6, 7]. Superradiance was recently demonstrated in diamond nanocrystals as well [8]. There are a few examples in the literature about that superradiance of emitters can be promoted by plasmonic nanoresonators, e.g. by concave and convex core-shell nanoparticles, and by complex structures as well [9-11]. It is an important scientific question, if it is possible to achieve superradiance via color centers coupled to plasmonic nanoresonators [12].

Methods

Core-shell type concave spherical plasmonic nanoresonators have been optimized to maximize the fluorescence rate of coupled dipolar emitters, namely SiV color centers in diamond. Four (4i) and six (6i) dipolar emitters simulating SiV color centers were arrayed along symmetrical square and hexagonal shaped patterns inside diamond-silver core-shell (SCS) and diamond-silver-diamond core-shell-shell (SCSS) type concave spherical nanoresonators.
The RF module of COMSOL Multiphysics was applied to extract the optical response and to analyze the near-field and charge distribution. Conditional optimization has been performed by an in-house developed GLOBAL optimization algorithm [13, 14]. The criterion regarding δR_{exc} radiative rate enhancement at the SiV excitation ensured that nanoresonators capable of enhancing the excitation were evaluated, while the criterion regarding *cQE* corrected quantum efficiency at the SiV emission was modified in multiple steps. The optimization was performed by selecting either the product of the radiative rate enhancements at the excitation and emission wavelengths nominated as P_x factor, or the product of the P_x**cQE* as the objective function.
To qualify the spherical nanoresonators the extinction (*ecs*) and scattering cross-section (*scs*) spectra (Figure 1a), while to qualify the achievable fluorescence enhancements the *Purcell factor* and *QE* quantum efficiency (Figure 1b and d) as well as the δR radiative rate enhancement (Figure 1c and e) have been determined as function of wavelength both in the excitation and emission configurations. The corresponding far-field radiation pattern, near-field and charge distributions were inspected at the SiV excitation and emission wavelength (not shown).

The radiative rate enhancements both at the excitation and at the emission were compared to the radiative rate enhancements of the corresponding reference systems consisting of one single dipole to inspect, if it is possible to achieve superradiance via multiple dipoles seeded nanoresonators (Figure 2a, Table 1). The enhancement of the FOMs, namely of the P_x and P_x*cQE was also determined, moreover the cQE corrected quantum efficiencies achievable in presence of multiple dipoles and a single dipole were compared as well (Figure 2a, Table 1, 2). The quality factor of the optimized resonators was computed based on the *ecs* extracted from plane wave illumination of nanoresonators with the specific geometry as well as based on the *Purcell factor* spectra (Figure 2b, Table 2). For the cooperatively oscillating emitters detuning of the *ecs* and *scs*, *Purcell factor* and δR radiative rate enhancement maxima from the SiV emission wavelength were determined (Table 2). The coupled systems were ranked taking into account all these quantities. Dependency of the two different FOMs on all geometrical parameters was inspected and compared for coupled systems optimized by applying the P_x and P_x*cQE objective functions (Figure 3 and 4). In addition to this the P_x*cQE was inspected as a function of both composing quantities, while the P_x was studied as a function of the cQE (Figure 5). The achievable P_x and P_x*cQE quantities were compared to uncover the advantages of different number of dipoles, different types of nanoresonators as well as different methods of optimizations.

Simulation Results and discussion

The geometrical parameters (*R, t, d*) of the optimized nanoresonators are very similar in case of 4 and 6 dipoles for the same SCS or SCSS nanoresonator types optimized with the same objective function (Figure 3, 4, Table 1). Namely, in SCS type nanoresonators optimized with P_x*cQE (P_x) the *R* core radius is ~33 nm (~30 nm), the *t* shell thickness is ~6 nm (~5 nm), which results in ~$9*10^{-1}$ *GAR* for both FOMs, whereas the *d* dipole distance is ~29 nm (~27 nm). Similarly, in SCSS type nanoresonators optimized with P_x*cQE (P_x) the *R* core radius is ~ 18 nm (~12 nm), the *t* shell thickness is ~7 nm (~5 nm), which corresponds to $7*10^{-1}$ *GAR* for both FOMs, while the dipole distance is ~13 nm (~8 nm).

The type of nanoresonators has more well defined effect, namely, independently of the method of optimization SCS type nanoresonators contain larger core, thinner shell (except in 4iSCS_ and SCSS_P_x), prefer larger dipole distances, and exhibit significantly larger GAR than the SCSS type resonators in case of 6 dipoles, (Figure 3 and 4).

The comparative study revealed that all geometrical parameters are larger in nanoresonators optimized with the P_x*cQE objective function, since the larger dipole distance allows reaching larger cQE in larger nanoresonators, while the *GAR* is similar to maintain resonance at the same wavelength (Figure 3 and 4). Accordingly, nanoresonators optimized to maximize P_x*cQE consist of a larger core, thicker shell, prefer larger dipole distances, but exhibit commensurate *GAR* compared to the parameters of nanoresonators optimized to maximize P_x (Figure 3 and 4).

The general characteristic of the optical signals from the nanoresonators is very similar. Although, the quantum efficiency is considerably larger throughout the complete inspected spectral interval, the radiative rate enhancement is larger (smaller) at the excitation (emission) in case of nanoresonators optimized by applying P_x*cQE as the objective function (Figure 1b-e). At the excitation wavelength the quantum efficiency is 66% and 65% (43% and 33%) in presence of 4 and 6 dipoles in SCS (SCSS) nanoresonators optimized with P_x*cQE. The QE is 60% and 59% (16% and 4%) in SCS (SCSS) nanoresonators consisting of 4 and 6 dipoles, which were optimized with P_x (Table 1). Moreover, the quantum efficiency at the excitation is larger in nanoresonators optimized with the P_x*cQE objective function, which proves the advantage of the composite objective function. Larger difference arises between the results from two different optimizations in case of SCSS type nanoresonators. The Purcell factor at the excitation is smaller in nanoresonators optimized with the P_x*cQE objective function, indicating that this objective function results in plasmonic nanoresonators, which are less strongly resonant at the excitation wavelength.

As a result, 4 and 6 (8 and 12)-fold δR radiative rate enhancement can be achieved at the excitation in presence of 4 and 6 dipoles in SCS (SCSS) nanoresonators optimized with P_x*cQE objective function. The 4 and 6 (8 and 11)-fold excitation enhancement is similar in the SCS (SCSS) nanoresonators optimized with P_x objective function (Table 1). The excitation rate enhancement is larger in nanoresonators optimized with the P_x*cQE objective function, which is in accordance with the larger achieved QE due to their larger size.

More significant emission enhancement can be achieved via all of the optimized nanoresonators. At the emission wavelength the cQE is 44% (40%), in presence of 4 and 6 dipoles in SCS (SCSS) nanoresonators optimized with P_x*cQE objective function. In contrast, the cQE is 38% (15%) in SCS (SCSS) nanoresonators consisting of 4 and 6 dipoles, which were optimized with P_x objective function (Table 1).

The quantum efficiency at the emission is larger in nanoresonators optimized with the P_x*cQE, similarly to the excitation, which proves the advantage of the composite objective function.

The *Purcell factor* is in the order of 10^3 (10^4) in SCS (SCSS) nanoresonators optimized with P_x*cQE objective function. Similar, but larger 10^3 and 10^4 (10^4) order of magnitude *Purcell factor* is achievable in presence of 4 and 6 dipoles in SCS (SCSS) nanoresonators optimized with P_x objective function (Table 1). The *Purcell factor* at the emission is smaller in nanoresonators optimized with the P_x*cQE, indicating that this objective function results in plasmonic nanoresonators, which are less strongly resonant at the emission wavelength as well.

As a result, $2*10^3$ and $4*10^3$ ($4*10^3$ and $7*10^3$) radiative rate enhancement can be achieved at the emission in presence of 4 and 6 dipoles in SCS (SCSS) nanoresonators optimized with P_x*cQE objective function. Similarly, the emission enhancement is $3*10^3$ and $4*10^3$ ($8*10^3$ and $1*10^4$) in SCS (SCSS) nanoresonators optimized with P_x objective function (Table 1). In contrast to the excitation, the emission rate enhancement is smaller in nanoresonators optimized with the P_x*cQE, which indicates that this objective function is less efficient to promote the emission enhancement.

Accordingly, $1*10^4$ and $2*10^4$ ($4*10^4$ and $8*10^4$) P_x factor can be achieved in presence of 4 and 6 dipoles in SCS (SCSS) type nanoresonators determined by applying P_x*cQE objective function. In comparison, $1*10^4$ and $3*10^4$ ($6*10^4$ and $1*10^5$) P_x factor can be achieved in presence of 4 and 6 dipoles in SCS (SCSS) nanoresonators determined by applying P_x objective function.

Finally, $4*10^3$ and $1*10^4$ ($2*10^4$ and $3*10^4$) P_x*cQE can be achieved in presence of 4 and 6 dipoles in SCS (SCSS) nanoresonators optimized with P_x*cQE objective function. Similarly, the P_x*cQE is $4*10^3$ and $1*10^4$ ($9*10^3$ and $2*10^4$) in SCS (SCSS) nanoresonators consisting of 4 and 6 dipoles, which were determined with P_x objective function (Table 1). In accordance with the intuitive expectation, the P_x*cQE (P_x) is larger in systems optimized with the P_x*cQE (P_x) objective function.

According to the radiative rate enhancement, larger (smaller) lobes correspond to the nanoresonators determined by applying the P_x*cQE objective function at the excitation (emission) wavelength (not shown). The amount of accumulated charges is significantly smaller in case of nanoresonators optimized with the P_x*cQE objective function, with one exception of 6iSCS at the excitation wavelength. This correlates with that the optimization with the P_x*cQE objective function results in nanoresonators playing with a weaker plasmonic resonance.

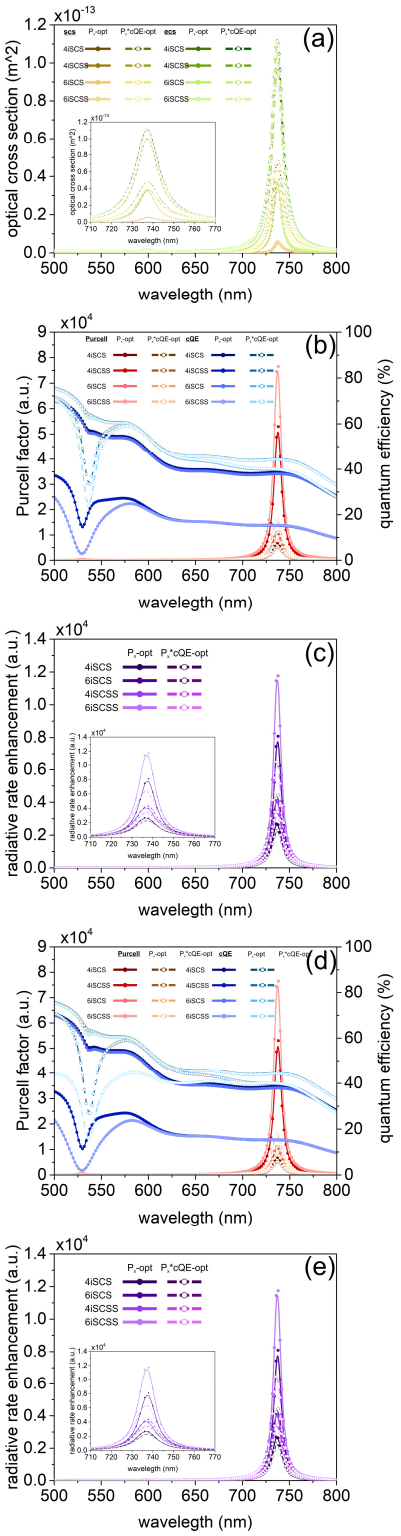

Figure 1. (a) Optical cross-sections, (b, d) quantum efficiency and Purcell factor, (c, e) raditative rate enhancement in (b, c) excitation and in (d, e) emission configuration as a function of wavelength.

Superradiance is achieved for the radiative rate enhancement at both wavelengths as well as for both FOMs in larger number of nanoresonators optimized with P_x*cQE objective function (Figure 2a, Table 2). The FWHM of the *ecs* and *scs*, *Purcell factor* and δR peaks are always larger in systems optimized with P_x*cQE objective function (Figure 2b, Table 2). This implies that the quality factor can be weaker in nanoresonators optimized to maximize P_x*cQE. Accordingly, the quality factor computed based on either of the *ecs* or the *Purcell factor* is always smaller in systems optimized with P_x*cQE objective function (Figure 2b, Table 2).

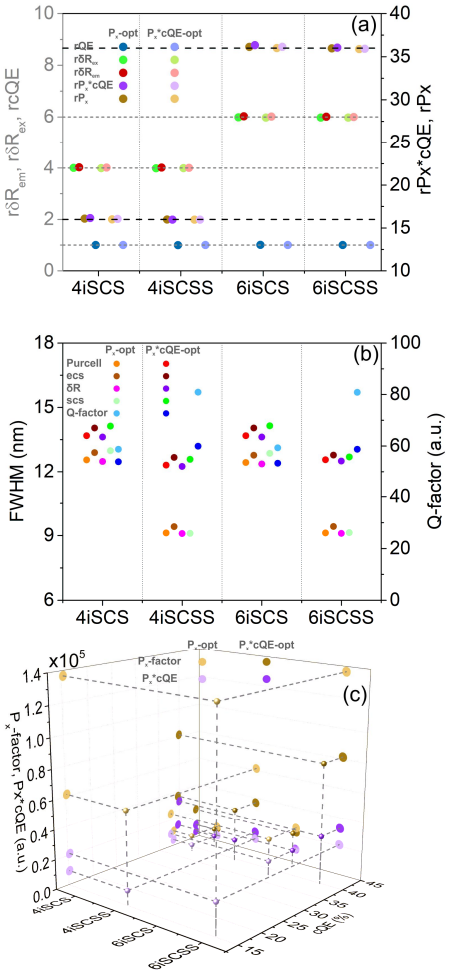

Figure 2. Ratios qualifying the degree of superradiance threshold overriding, FWHMs and the corresponding Q-factors, P_x and P_x*cQE for different systems as a function of accompanying cQE.

The P_x objective function is capable of resulting in significantly larger quality factor, the enhancement with respect to the counterpart nanoresonators optimized with P_x*cQE objective function is larger in case of 4 dipoles and in case of SCSS nanoresonators. This indicates again that the main advantage of the optimization performed by applying the P_x objective function arises in non-cooperative fluorescence enhancement (Figure 2b, Table 1, 2).

However, to achieve plasmonic Dicke effect (PDE) operation the bad-cavity region is preferred, therefore the nanoresonators optimized with the P_x*cQE objective function are proposed. The achieved larger cQE makes it possible that the systems optimized to maximize P_x*cQE are better in superradiance achievement than the systems optimized to maximize the P_x (Figure 2b, c, Table 1, 2). This is due to that the QE is inversely proportional to the *Purcell factor*, which includes the quality factor, as a result by maximizing a composite objective function consisting of cQE, one moderates the Q, which is the precondition of plasmonic Dicke effect.

Detuning of the *ecs* peak from the emission is smaller (larger) in 4iSCS, 6iSCS and 6iSCSS (4iSCSS), while for *scs* detuning is smaller (larger) in 4&6iSCSS (4&6iSCS) systems optimized to maximize P_x*cQE (Table 2). Detuning of the *Purcell factor* and δR peak from the emission is smaller (larger) in 4iSCSS and 6iSCS (4iSCS and 6iSCSS) systems optimized to maximize P_x*cQE (Table 2).

Inspection of the figure of merits (FOM) as a function of nanoresonator geometrical parameters for all the systems received via conditional optimizations (Figure 3 and 4), and the P_x*cQE composite FOM as a function of both composing quantities as well as the P_x as a function of cQE proved the reliability of the objective functions (Figure 5). Although, the fitting has been performed for the nanoresonators determined by different objective functions independently, the fitted curves overlap for the corresponding systems. The P_x*cQE FOM indicates a global maximum as a function of all geometrical parameters (R, t, GAR) in all nanoresonators optimized by applying the P_x*cQE objective function, except the 6iSCSS, which exhibits a maximum outside the inspected parameter interval in R and t parameters (Figure 3).

Similarly, among the nanoresonators determined by applying the P_x objective function the 4iSCSS and 6iSCSS exhibit a global maximum in P_x*cQE inside the intervals of representative points for all inspected geometrical parameters. In contrast, the maxima are taken on outside these intervals in R, t and GAR dependency of 6iSCS and in R dependency of 4iSCS, while the t and GAR dependency does not show a maximum (Figure 3). The intervals, where the P_x*cQE takes on the global maximum in R / t / GAR parameters are bounding / overlapping / different for SCS and SCSS nanoresonators (Figure 3).

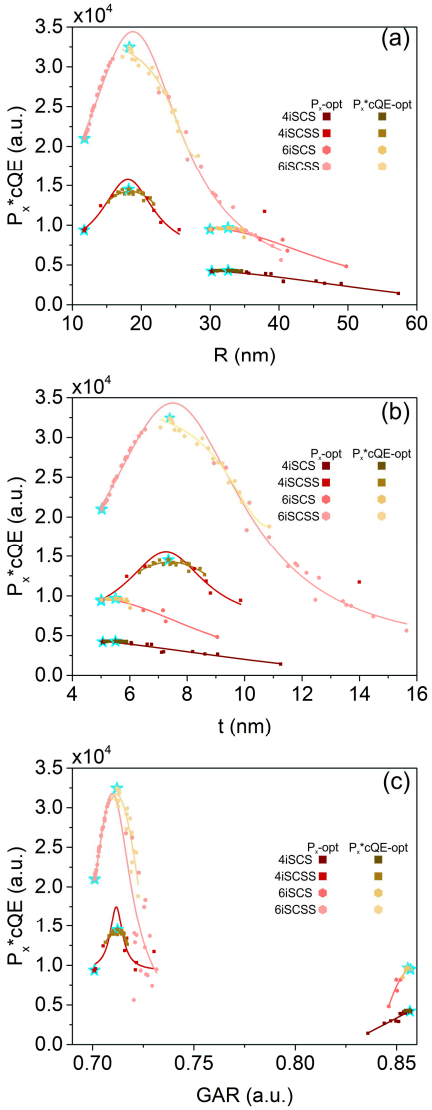

Figure 3. The P_x*cQE FOM as a function of the (a) R radius of the core, (b) t thickness of the shell and (c) GAR generalized aspect ratio of the nanoresonator.

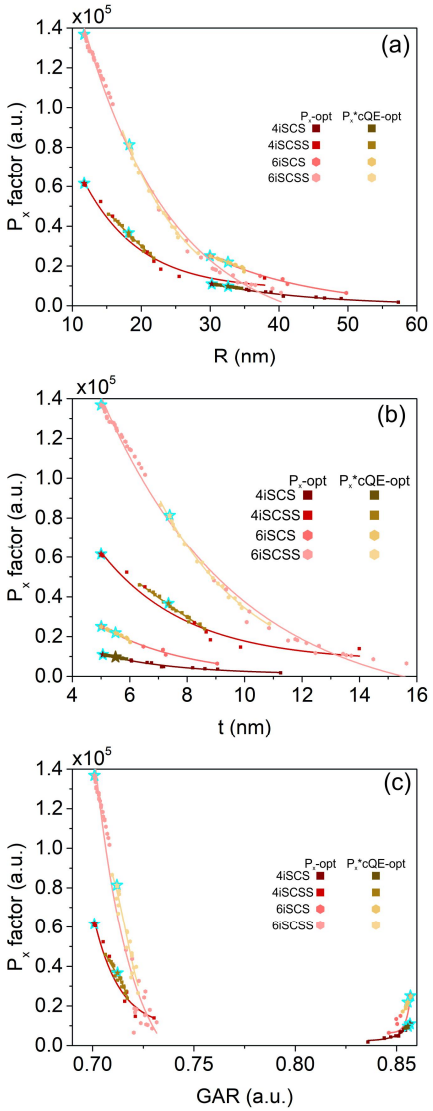

Figure 4. The P_x FOM as a function of the (a) R radius of the core, (b) t thickness of the shell and (c) GAR generalized aspect ratio of the nanoresonator.

In contrast, the P_x quantity almost monotonously modifies throughout the inspected geometrical parameter intervals (Figure 4). The fitted functions take on larger values for 6 dipoles than for 4 dipoles for both FOMs as a function of all geometrical parameters (Figure 3 and 4). The tendencies are more pronounced in case of SCSS nanoresonators. The fitted functions take on larger values for SCSS type resonators than for SCS resonators for both FOMs as a function of all geometrical parameters (Figure 3 and 4). The P_x*cQE FOM is larger in the systems optimized with the P_x*cQE, than in the systems optimized with P_x (Figure 3).

In contrast, among the nanoresonators determined by applying the P_x objective function only the 4iSCSS and 6iSCSS exhibit a global maximum in P_x*cQE as a function of both composing quantities, while 4iSCS and 6iSCS exhibit a global maximum in cQE outside the interval of representative points (Figure 3). Moreover, the P_x*cQE FOM indicates a global maximum as a function either of the P_x or the cQE as well in all nanoresonators optimized by applying the P_x*cQE objective function (Figure 5a, b). Only the 6iSCSS takes on the maximum outside the inspected cQE interval. In contrast, the P_x exhibits exponential decay as a function of the cQE, independently of the optimization method (Figure 5c).

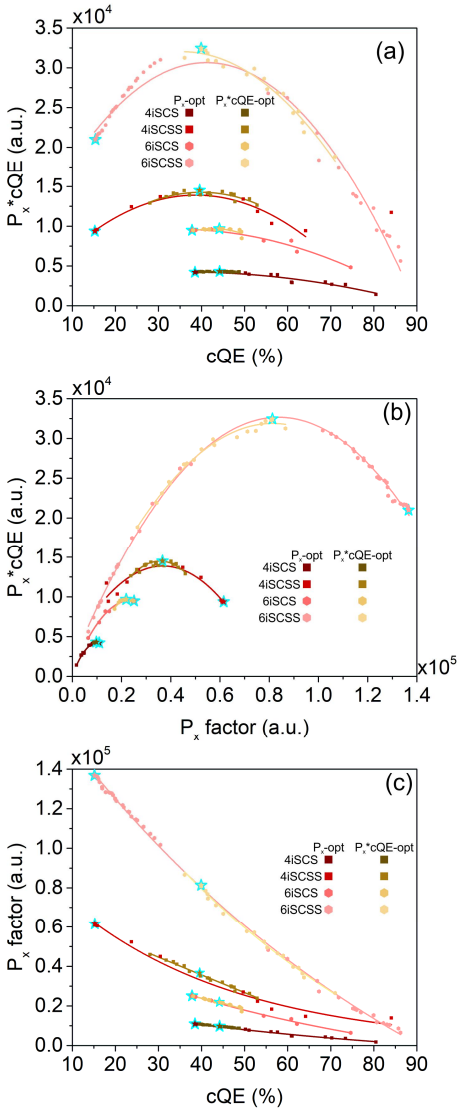

Figure 5. The P_x*cQE FOM as a function of the composing quantities: (a) cQE corrected quantum efficiency, (b) P_x complete fluorescence enhancement. (c) The P_x FOM as a function of the cQE.

The ranking of nanoresonators optimized by applying P_x*cQE objective function results in the order of 6iSCS>6iSCSS>4iSCS>4iSCSS, while in case of nanoresonators optimized by applying P_x the ranking results in order of 6iSCSS>6iSCS=4iSCS>4iSCSS.

Conclusions

The optimization by applying P_x*cQE results in bad-cavity-type nanoresonators for superradiance, while good-cavities for non-cooperative fluorescence enhancement can be designed by applying the P_x.

Accordingly, the presented results indicate that the main advantages of the optimization performed by applying the P_x*cQE (P_x) objective function manifest themselves in significant cooperative (non-cooperative) fluorescence enhancement. The provided numerical methodology can be applied to design and optimize superradiant systems, until when the coupling between the sparse arrays of emitters through the plasmonic modes is dominant.

Table 1. Geometrical parameters and optical responses of optimized systems: R – core radius, t – shell thickness, d – dipole distances from shell, GAR – generalized aspect ratio, $P_{exc/em}$ – Purcell factor, QE_{exc} – quantum efficiency at excitation, cQE_{em} – corrected quantum efficiency at emission, $\delta R_{exc/em}$ – radiative rate enhancement, $charge_{exc/em}$ – accumulated charge, P_x – P_x factor, P_x*cQE objective function to achieve superradiance, rP_x and rP_x*cQE enhancements with respect to reference systems.

system	opt	R (nm)	t (nm)	d (nm)	GAR (nm)
4iSCS	P_x*cQE	32.61	5.5	29.44	0.8556
	P_x	30.24	5.06	26.88	0.8566
4iSCSS	P_x*cQE	18.2	7.35	13.64	0.7123
	P_x	11.73	5	9.1	0.7009
6iSCS	P_x*cQE	32.59	5.5	28.87	0.8555
	P_x	29.97	5.01	26.53	0.8568
6iSCSS	P_x*cQE	18.28	7.39	12.96	0.712
	P_x	11.78	5.02	7.3	0.701
system	opt	P_{exc}	QE_{exc}	δR_{exc}	$charge_{exc}$
4iSCS	P_x*cQE	6.35	66.26	4.21	2.29E-16
	P_x	6.79	59.7	4.05	3E-16
4iSCSS	P_x*cQE	19.35	42.69	8.26	3.63E-15
	P_x	46.69	16.14	7.54	5.96E-15
6iSCS	P_x*cQE	9.69	65.03	6.3	4.83E-16
	P_x	10.28	58.8	6.04	4.65E-16
6iSCSS	P_x*cQE	38.03	32.69	12.43	7.48E-15
	P_x	324.29	3.47	11.26	2.58E-14
system	opt	P_{em}	cQE_{em}	δR_{em}	$charge_{em}$
4iSCS	P_x*cQE	5.24E+03	44.19	2.32E+03	4.55E-14
	P_x	7.03E+03	38.46	2.70E+03	5.25E-14
4iSCSS	P_x*cQE	1.12E+04	39.57	4.44E+03	1.57E-13
	P_x	5.36E+04	15.22	8.16E+03	3.4E-13
6iSCS	P_x*cQE	7.87E+03	44.15	3.47E+03	6.82E-14
	P_x	1.10E+04	37.8	4.15E+03	8.06E-14
6iSCSS	P_x*cQE	1.64E+04	39.91	6.54E+03	2.32E-13
	P_x	7.90E+04	15.36	1.21E+04	5.07E-13
system	opt	P_x	P_x*cQE	rP_x	rP_x*cQE
4iSCS	P_x*cQE	9.75E+03	4.31E+03	16.07	16.15
	P_x	1.10E+04	4.21E+03	15.99	16.04
4iSCSS	P_x*cQE	3.66E+04	1.45E+04	15.97	15.96
	P_x	6.15E+04	9.36E+03	15.95	15.95
6iSCS	P_x*cQE	2.20E+04	9.67E+03	36.13	36.33
	P_x	2.51E+04	9.48E+03	36	36.12
6iSCSS	P_x*cQE	8.13E+04	3.25E+04	35.95	36.04
	P_x	1.37E+05	2.10E+04	35.88	35.91

Table 2. Optical responses of optimized systems: $rcQE_{em}$ and $r\delta R_{exc/em}$ – enhancements with respect to reference systems; location, detuning, FWHM of P_{exc}, δR_{exc}, extinction and scattering cross-sections peaks, and the corresponding Q quality factor.

system	opt	$rcQE_{em}$		$r\delta R_{exc}$	$r\delta R_{em}$
4iSCS	P_x*cQE	1.005		4	4.02
	P_x	1.0031		3.99	4.01
4iSCSS	P_x*cQE	0.9994		3.98	4.01
	P_x	1		3.99	4
6iSCS	P_x*cQE	1.0055		5.99	6.03
	P_x	1.0033		5.98	6.02
6iSCSS	P_x*cQE	1.0025		5.98	6.01
	P_x	1.0008		5.98	6
system	opt	P_{em} : Purcell factor at emission			
		Location (nm)	Detuning (nm)	FWHM (nm)	Q factor
4iSCS	P_x*cQE	737.27	0.27	13.68	53.89
	P_x	736.79	-0.21	12.55	58.71
4iSCSS	P_x*cQE	737.46	0.46	12.31	59.91
	P_x	737.78	0.78	9.12	80.90
6iSCS	P_x*cQE	737.02	0.02	13.68	53.88
	P_x	736.97	-0.03	12.43	59.29
6iSCSS	P_x*cQE	737.46	0.46	12.56	58.71
	P_x	737.14	0.14	9.12	80.83
system	opt	δR_{em} radiative rate enhancement at emission			
		Location (nm)	Detuning (nm)	FWHM (nm)	Q factor
4iSCS	P_x*cQE	737.26	0.26	13.62	54.13
	P_x	736.79	-0.21	12.48	59.04
4iSCSS	P_x*cQE	737.42	0.42	12.25	60.20
	P_x	737.46	0.46	9.09	81.13
6iSCS	P_x*cQE	737.01	0.01	13.62	54.11
	P_x	736.67	-0.33	12.36	59.60
6iSCSS	P_x*cQE	737.43	0.43	12.50	58.99
	P_x	737.13	0.13	9.10	81.00
system	opt	extinction cross section (ecs)			
		Location (nm)	Detuning (nm)	FWHM (nm)	Q factor
4iSCS	P_x*cQE	737.22	0.22	14.04	52.49
	P_x	736.66	-0.34	12.89	57.13
4iSCSS	P_x*cQE	737.44	0.44	12.67	58.13
	P_x	737.19	0.19	9.41	78.37
6iSCS	P_x*cQE	737.03	0.03	14.04	52.48
	P_x	736.61	-0.39	12.77	57.66
6iSCSS	P_x*cQE	736.95	-0.05	12.78	57.68
	P_x	737.15	0.15	9.42	78.23
system	opt	scattering cross section (scs)			
		Location (nm)	Detuning (nm)	FWHM (nm)	Q factor
4iSCS	P_x*cQE	737.65	0.65	14.13	52.20
	P_x	737.06	0.6	12.98	56.78
4iSCSS	P_x*cQE	738.23	1.23	12.58	58.68
	P_x	738.29	1.29	9.1	81.13
6iSCS	P_x*cQE	737.46	0.46	14.14	52.15
	P_x	737.01	0.01	12.86	57.31
6iSCSS	P_x*cQE	737.75	0.75	12.69	58.14
	P_x	738.24	1.24	9.13	80.86

References

[1] Hutter, E. & Fendler, J. H., Exploitation of Localized Surface Plasmon Resonance, *Adv. Mater.* **16** (19), 1685-1706 (2004)

[2] Prodan, E., Lee, A. & Nordlander, P., The effect of a dielectric core and embedding medium on the polarizability of metallic nanoshells, *Chem. Phys. Lett.* **360**, 325-332 (2002)

[3] Aharonovich, I. & Neu, E., Diamond Nanophotonics, *Adv. Opt. Mater.* **2** (10), (2014)

[4] Hepp, C. et. al., Electronic Structure of the Silicon Vacancy Color Center in Diamond, *Phys. Rev. Lett.* **112**, 036405 (2014)

[5] Dicke, R. H. Coherence in spontaneous radiation processes, *Phys. Rev.* **93** (1), 99 (1954).

[6] Rehler, N. E. & Eberly, J. H., Superradiance, *Phys. Rev. A*, **3**, 1735 (1971)

[7] Andreev, A. V., Emel'yanov, V. I. & Il'inskiĭ, Y. A., Collective spontaneous emission (Dicke superradiance), *Sov. Phys. Usp.* **23**, 493-514 (1980)

[8] Bradac, C. et. al., Observation of room-temperature spontaneous superradiance from single diamond nanocrystals. *Nat. Commun.* **8** (1), 1205 (2017)

[9] Pustovit, V. N. & Shahbazyan, T. V. Plasmon-mediated superradiance near metal nanostructures, *Phys. Rev. B* **82**, 075429 (2010)

[10] Manassah, J. T., The Purcell-Dicke effect in the emission from a coated small sphere of resonant atoms placed inside a matrix cavity, *Laser Phys.* **22** (4), 738-744 (2012)

[11] Dorofeenko, A. V. et. al., Steady state superradiance of a 2D-spaser array, *Opt. Express,* **21** (12), 14539-14547 (2013)

[12] Vass, D., Szenes, A., Bánhelyi, B., Csendes, M., Szabó, G. & Csete, M. Superradiant diamond color center arrays coupled to concave plasmonic nanoresonators, arXiv:1807.03248 (2018)

[13] Csendes, T., Pál, L., Sendin, J. O. H. & Banga, J. R. The GLOBAL optimization method revisited. *Optim. Lett.* **2**, 445-454 (2008)

[14] Bánhelyi, B., Csendes, T., Lévai, B., Pál, L. & Zombori, D. The GLOBAL optimization algorithm. Newly Updated with Java Implementation and Parallelization. *Springer Briefs on Optimization,* accepted (2018)

Acknowledgements

The research was supported by the National Research, Development and Innovation Office-NKFIH through project “Optimized nanoplasmonics” K116362. The project has been supported by the European Union, co-financed by the European Social Fund. EFOP-3.6.2-16-2017-00005. The authors are grateful to Tamás Dániel Juhász for coding of some related programs. Tamás Dániel Juhász was supported by EFOP-3.6.3-VEKOP-16-2017-0002.